Progress in Nuclear Energy 94 (2017) 126–132

Contents lists available at ScienceDirect

Progress in Nuclear Energy

journal homepage: www.elsevier.com/locate/pnucene

Neutron transmission and capture measurements and analysis of Dy from 0.01 to 550 eV

R.C. Block [a, *], M.C. Bishop [a, e], D.P. Barry [a], G. Leinweber [a], R.V. Ballad [a, 1], J.A. Burke [a], M.J. Rapp [a], Y. Danon [b], A. Youmans [b], N.J. Drindak [a, 1], G.N. Kim [c], Y.-R. Kang [d], M.W. Lee [d], S. Landsberger [e]

[a] Bechtel Marine Propulsion Corp., Knolls Atomic Power Laboratory, P.O. Box 1072, Schenectady, NY 12301-1072, United States
[b] Rensselaer Polytechnic Institute, Gaerttner LINAC Center, 110 8th St., Troy, NY 12180, United States
[c] Department of Physics, Kyungpook National University, Daegu 702-701, Republic of Korea
[d] Research Center, Dongnam Inst. of Radiological & Medical Sciences, Busan 619-953, Republic of Korea
[e] University of Texas at Austin, Nuclear Engineering Teaching Lab, Pickle Research Campus, R-9000, Austin, TX 78712, United States

ARTICLE INFO

Article history:
Received 14 March 2016
Received in revised form
9 September 2016
Accepted 28 September 2016

Keywords:
Dysprosium
Resonance parameters
Dy164 thermal cross section
Dy164 resonance integral

ABSTRACT

Neutron capture and transmission measurements were carried out from 0.01 to over 600 eV on both natural Dy and samples highly enriched in ^{164}Dy. These data were analyzed for resonance parameters utilizing the SAMMY Bayesian analysis code to simultaneously fit both the capture and transmission data. Parameters were obtained for 17 resonances in Dy isotopes up to 18 eV and for the ^{164}Dy resonances near 147, 450 and 540 eV. The thermal capture cross section (at 0.0253 eV) and capture resonance integral were determined for ^{164}Dy.

1. Introduction

Natural dysprosium has a high neutron thermal capture cross section of 950 b, of which approximately 80% is from capture in ^{164}Dy. Since ^{164}Dy is produced inside a reactor as a fission product or it can be used as a burnable poison to control a reactor (Raaijmakers, 1965), it is important to know the ^{164}Dy cross section accurately over the energy range of neutrons inside a reactor. Total cross section measurements in the thermal energy region have been reported by Sher et al. (1961), Moore (1961), and Vertebnyj et al. (1971). Earlier cross section measurements of Dy isotopes in the resonance region have been reported by Mughabghab and Chrien (1970) (transmission) and Liou et al. (1975) (transmission and capture). Kim et al. (2003). measured a single 0.5-mm thick sample of natural Dy in transmission at 10.8 m and reported resonance parameters below 10 eV. However, these measurements used thick samples of Dy which made it difficult to obtain accurate information on the large ^{164}Dy resonances. It was thus decided to carry out a new set of measurements with samples over an order of magnitude thinner than used in the earlier measurements. These thinner samples were also well suited for measurements in the thermal energy region.

Neutron capture and transmission measurements were thus carried out at the Rensselaer Polytechnic Institute (RPI) Gaerttner LINAC Center from 0.01 to over 600 eV on both natural Dy and samples highly enriched in ^{164}Dy. Both metallic and liquid samples were employed for these measurements. Resonance parameters were deduced for resonances in the Dy isotopes up to 18 eV and for the ^{164}Dy resonances near 147, 450 and 540 eV. The thermal capture cross section (at 0.0253 eV) and the capture resonance integral for ^{164}Dy were determined from these parameters.

2. Experimental conditions

2.1. Overview of measurements

Transmission and capture measurements were carried out using the time-of-flight (TOF) method predominantly with samples

* Corresponding author.
E-mail address: blockr@rpi.edu (R.C. Block).
[1] Retired.

http://dx.doi.org/10.1016/j.pnucene.2016.09.019
0149-1970/

highly enriched in ^{164}Dy. The experimental details used for data acquisition are listed in Table 1. The experimental method and details are essentially the same as those reported in detail by Leinweber et al. (2014) and will only be briefly described here. The RPI Gaerttner LINAC Center linear accelerator was used to produce energetic electrons and these electrons, in turn, impinged on water-cooled Ta plates to produce neutrons via the photoneutron reaction. The thermal transmission and capture measurements used the enhanced thermal neutron target (Danon et al., 1993, 1995) whereas the epithermal transmission and capture measurements used the bare bounce target (Overberg et al., 1999). The thermal transmission measurements utilized a 0.3-cm-thick ^{6}Li glass scintillator detector mounted directly on a photomultiplier at the 15 m flight station. The epithermal transmission measurements utilized a 1.27-cm-thick (0.5 in) ^{6}Li glass detector at the 25 m flight station with the glass viewed by two photomultipliers located outside of the neutron beam (Barry, 2003). The thermal and epithermal capture measurements utilized the 16-section NaI multiplicity detector (Block et al., 1988) located at the 25 m flight station.

The neutron intensity from the accelerator was monitored with moderated fission chambers located at a ≈9 m flight path, a ^{6}Li glass ring detector placed in the epithermal transmission flight tube and, when applicable, the ^{6}Li glass detector located at the 15 m flight path. These monitor detectors were used to remove the effects of beam intensity fluctuations, as well as correct for different collection times for the various sample and open positions.

2.2. Sample information

The natural dysprosium sample and the enriched 164 isotope material for the liquid samples were obtained from Trace Sciences International. The metallic enriched ^{164}Dy sample was supplied by Kyungpook National University in the Republic of Korea. Several types of samples were used for these measurements; Table 2 lists the sample thicknesses (elemental number densities) and Table 3 lists the isotopic compositions of the enriched samples. The uncertainties in the isotopic compositions of the enriched and natural samples are estimated as ±1 atom percent.

2.2.1. Solid samples

The 10 mil Dy sample (1 mil = 0.001in = 0.00254 cm) was a natural metal sample and was used for measuring Dy capture in both the thermal and epithermal neutron energy regions and transmission in the epithermal region. For capture measurements this sample was enclosed in an empty quartz cell (the same type cell used for the liquid samples) so that the incident flux on the 10 mil sample is the same as the flux on the liquid samples. The 20 mil Dy sample was used for the thermal transmission measurement. The uncertainty in the number density was estimated at ±1% for these samples.

The ^{164}Dy metal sample was used in the Week 3 epithermal capture measurement. It was somewhat irregularly shaped, so the uncertainty in its number density was estimated at ±11%.

Table 1
Experimental details showing accelerator and data acquisition parameters.

Measurement	Overlap filter	Neutron target	Electron pulse width (μs)	Average electron current (μA)	Electron energy (MeV)	Neutron energy region (eV)	Channel width (μs)	Rep. Rate (pps)	Flight path (m)
Thermal transmission	none	Enhanced thermal	2.1	10.5	48	E < 0.11 0.11 < E < 5.3 5.3 < E < 24	32 2 0.5	25	14.973 ± 0.006
Epithermal transmission	Cd	Bare bounce	0.060	20.5	54	E < 45 44.7 < E < 262 262 < E < 600	0.5 0.0625 0.03125	225	25.597 ± 0.006
Thermal capture	none	Enhanced thermal	1.0	8.2	50	E < 0.12 0.12 < E < 4.0 4.0 < E < 23	8 0.5 0.125	25	25.444 ± 0.006
Epithermal capture (week 1)	Cd	Bare bounce	0.044	14.5	55	E < 45 44.7 < E < 262 262 < E < 600	0.5 0.0625 0.03125	225	25.564 ± 0.006
Epithermal capture (week 2)	Cd	Bare bounce	0.036	14	60	E < 45 44.7 < E < 262 262 < E < 600	0.5 0.0625 0.03125	225	25.564 ± 0.006
Epithermal capture (week 3)	B_4C	Bare bounce	0.018	17.2	58	E < 1000	0.0128	225	25.564 ± 0.006

Table 2
Sample thicknesses as elemental number densities in atoms per barn. The ^{164}Dy metal sample was produced from material highly enriched in ^{164}Dy; LX-15 and LX-22 contained pure D_2O and were used as compensator samples in the transmission measurements. The other LX samples were solutions containing enriched ^{164}Dy, D_2O, remnants of deuterated nitric acid (used in sample preparation), and H_2O that was inadvertently picked up during the preparation.

Sample	^{164}Dy	Elemental number densities				
	Enrichment (%)	Dy (a/b)	D (a/b)	N (a/b)	O (a/b)	H (a/b)
Dy natural metal (10 mil)	28.18	8.05E-04				
Dy natural metal (20 mil)	28.18	1.61E-03				
Dy-164 metal	98.45	2.27E-04				
LX-12	98.60	8.59E-05	2.45E-02	4.16E-04	1.34E-02	1.84E-04
LX-13	98.60	2.20E-04	2.20E-02	1.06E-03	1.40E-02	4.69E-04
LX-14	98.60	5.57E-04	1.63E-02	2.70E-03	1.57E-02	1.19E-03
LX-15			2.62E-02		1.31E-02	
LX-18	98.60	1.48E-05	1.04E-02	7.15E-05	5.40E-03	3.15E-05
LX-19	98.60	3.54E-05	1.01E-02	1.72E-04	5.52E-03	7.56E-05
LX-21	98.60	2.29E-04	7.23E-03	1.11E-03	6.78E-03	4.90E-04
LX-22			1.09E-02		5.43E-03	
LX-23	98.60	9.06E-05	9.08E-03	4.39E-04	5.77E-03	1.94E-04

Table 3
Isotopic composition (in atom percent) of the LX series (liquid samples) and metallic samples.

Enriched sample	^{156}Dy (%)	^{158}Dy (%)	^{160}Dy (%)	^{161}Dy (%)	^{162}Dy (%)	^{163}Dy (%)	^{164}Dy (%)
LX Series			0.01	0.09	0.22	1.08	98.60
Dy-164 metal	<0.01	<0.02	0.02	0.15	0.35	1.03	98.45
Dy natural metal	0.06	0.1	2.34	18.91	25.51	24.90	28.18

2.2.2. Liquid samples

It is a problem to produce uniformly thin solid samples. Metallic samples thinner than ≈0.005 in (0.0127 cm) and powdered samples thinner than ≈0.020 in (0.0508 cm) are difficult, if not impossible, to produce with a uniform thickness. It is, however, possible to produce uniformly thin liquid samples. Thus liquid samples were prepared, and these are listed as the LX samples in Table 2. The LX samples contained either ^{164}Dy in solution or pure D_2O. The D_2O samples were used as compensating samples for the transmission measurements. Note that there is more D in the D_2O samples than in the Dy samples; this is taken into account when analyzing the transmission data.

The ^{164}Dy liquid samples were prepared by dissolving enriched dysprosium oxide (Dy_2O_3) in deuterated nitric acid (DNO_3) and then diluting with heavy water (D_2O) to achieve the desired dysprosium concentrations (Ernesti, 2008). Although great care was taken to minimize any light water (H_2O) from entering the solution it was determined that a small amount was apparently picked up during sample preparation. Since H has a high total cross section of ≈20 b, this small amount of H_2O had to be accounted for in the transmission measurements. The uncertainties in the nuclear number densities are estimated as ±2% for the liquid samples.

The liquid samples were enclosed in 1.5-in-dia. (3.81 cm) quartz cells with 1/32-in-thick (0.0794 cm) windows. This window thickness was selected to minimize the effect of neutron scattering in the windows and the effect of this scattering upon the capture measurements. It was determined via Monte Carlo calculations that this scattering effect on the capture in the ^{164}Dy was less than ~1% and could be neglected when analyzing these measurements. Four dysprosium concentrations and two thicknesses of liquids, 0.397 cm (5/32 in) and 0.159 cm (1/16 in), were employed to cover the range of number densities needed for these measurements.

2.3. Transmission and capture measurements

The 'thermal' measurement consisted of two sets of measurements: a transmission measurement with four samples and a capture measurement with four samples. The 'epithermal' transmission measurement was done in one set of measurements utilizing four samples while the epithermal capture measurements with the liquid samples were done in two separate measurements in weeks 1 and 2, each with four samples. The highly-enriched metallic ^{164}Dy sample was measured in a separate set of capture measurements (which did not include the liquid samples) during week 3. Table 3 lists the isotopic compositions and Table 4 lists the combination of liquid and natural Dy and ^{164}Dy metal samples used in these measurements.

3. Data reduction

The method for the reduction of the transmission and capture data was essentially the same as carried out by Leinweber et al. (2014). The capture data were reduced to capture yield and the transmission data to transmission.

Table 4
The liquid, natural Dy (10 and 20 mil metal) and ^{164}Dy metal samples used in the thermal (th) and epithermal (epi) transmission and capture measurements.

Measurement	Samples			
Transmission (th)	LX-12	LX-13	LX-14	Dy natural metal (20 mil)
Capture (th)	LX-12	LX-13	LX-19	Dy natural metal (10 mil)
Transmission (epi)	LX-12	LX-13	LX-14	Dy natural metal (10 mil)
Capture (epi) Week 1	LX-19	LX-21	LX-23	Dy natural metal (10 mil)
Capture (epi) Week 2	LX-18	LX-19	LX-23	Dy natural metal (10 mil)
Capture (epi) Week 3				^{164}Dy metal

3.1. Neutron energy

The neutron energy at low (non-relativistic) energies in time-of-flight channel i is given by

$$E_i = \left[\frac{72.296L}{t_i - t_0}\right]^2 \quad (1)$$

where E_i is the energy in eV, L is the flight path length in meters, and $(t_i\text{-}t_o)$ is the time-of-flight in μs. The recorded time of an event in channel i is t_i while t_o is the time when the electron pulse strikes the neutron target. By measuring the time when the 'gamma flash' is detected, t_o is obtained by correcting for the flight time of these gamma rays from the neutron target to the detector.

3.2. Capture yield

The capture yield Y_i in TOF channel i is calculated by

$$Y_i = \frac{C_i - B_i}{K\,\varphi_{r,i}} \quad (2)$$

where the numerator refers to the net capture counting rate with the capture sample in the beam and the denominator to the neutron rate incident upon the capture sample. C_i and B_i are, respectively, the dead-time-corrected counting rate with the capture sample in the beam and the background counting rate without a sample in the beam. The relative neutron flux incident upon the capture sample $\varphi_{r,i}$ was determined from a measurement with a $^{10}B_4C$ sample placed in the neutron beam where the counting data are dead-time corrected, background subtracted, and the resulting net counting data are divided by the efficiency for detecting the gamma ray from the ^{10}B (n; α,γ) reaction. The constant K normalizes the relative neutron flux to the actual neutron rate incident upon the capture sample.

The normalization constant K is typically determined by measuring capture in a region where the capture yield Y is best known. If the sample has a black, saturated resonance which is mostly capture, the yield is approximately equal to unity and K can be obtained from Eq. (2). If there is no saturating resonance then a resonance which is well known, e.g., a low energy resonance measured in transmission with accurately measured radiation and neutron widths, can be used to obtain K. The area under the

resonance in capture can be normalized to the area calculated from the resonance parameters. There is no black saturated resonance in ^{164}Dy. There is, however, a mostly capture resonance in ^{162}Dy at 5.45 eV that saturates in the 10 mil Dy capture measurement; this was used to determine K for capture in ^{162}Dy. The epithermal capture yield in the metallic enriched ^{164}Dy sample (epithermal capture week 3) was normalized using the resonance parameters at the 147 eV resonance derived from the liquid enriched (in ^{164}Dy) and natural metallic samples. The uncertainty in the normalization of the epithermal capture yield in the metallic enriched ^{164}Dy sample is estimated to be ±5%.

The efficiencies for capture in the other isotopes of Dy differ from that for ^{162}Dy and this must be accounted for in analyzing the data based on a flux normalized to capture in ^{162}Dy. These efficiencies were determined from the efficiency variations in a similar set of nuclei. Capture detector efficiencies for capture in ^{149}Sm, an even-odd nucleus, and ^{150}Sm, an even-even nucleus, were determined from capture gamma ray cascade calculations and subsequent transport and capture into the 16-section NaI multiplicity detector (Wang et al., 2003). The efficiency was determined as a function of binding energy and discriminator setting (for total energy deposit in all 16 sections) for both nuclei. The efficiencies for capture in the odd-even and even-even Dy isotopes were first set equal to these Sm efficiencies. However, it turned out that the odd-even Dy efficiencies did not quite fit the thermal capture measurements of the low energy ^{161}Dy and ^{163}Dy resonances. The odd-even Dy efficiencies (for thermal measurements) were then renormalized to capture in the 1.71 eV ^{163}Dy resonance.

The final Dy capture efficiencies for epithermal (total energy discriminator at 1 MeV) and thermal (total energy discriminator at 2 MeV) capture, along with their estimated uncertainties, are listed in Table 5. The epithermal efficiencies range from 97% for ^{161}Dy and ^{163}Dy to 87% for ^{164}Dy, a variation of 10%. The thermal efficiencies range from 91% to 78%, a variation of 13%.

3.3. Transmission

The neutron transmission T_i in TOF channel i is given by

$$T_i = \frac{C_i^S - K_S B_i - B_S}{C_i^O - K_O B_i - B_O} \quad (3)$$

where C_i^S and C_i^O are the dead-time-corrected and monitor-normalized counting rates for the sample and open measurements, respectively; B_i is the un-normalized time-dependent background counting rate; B_S and B_O are the steady-state background counting rates for the sample and open measurements, respectively; and K_S and K_O are time-dependent background normalization factors for the sample and open measurements, respectively.

The determination of the time-dependent background is one of the more difficult tasks to accomplish. This background was determined by cycling a set of samples with blacked-out resonances, called 'notches', and extrapolating to the sample and open conditions without the notch samples in the beam. For the epithermal transmission measurements a 0.104 cm (0.041-in-thick) Mn-Cu alloy (80%Mn-20%Cu) sample was left permanently in the beam to provide a notch near 330 eV. Samples of Ag, Co and W were placed in the beam during the notch measurements to produce notches, respectively, near 5.2, 18.6 and 132 eV. For the thermal measurements a 0.005-in-thick (0.0127 cm) W sample was left permanently in the beam to produce a notch near 18.6 eV, and a package of Cd, In, and Ag samples was cycled into the beam to provide notches, respectively, below 0.3 eV and near 1.45 and 5.2 eV.

4. Results

The transmission and capture data were analyzed for resonance parameters using the R-matrix Bayesian code SAMMY version 8 (Larson, 2008). The analysis employed the experimental resolution, Doppler broadening, self-shielding, multiple scattering, and Reich-Moore approximation features of SAMMY. This code takes into account the statistical fluctuations in the experimental data points and known uncertainties in experimental parameters such as sample thickness, detector efficiency, flight path length, etc. Both the transmission and capture yield data were fitted and a final set of resonance parameters was obtained for the best overall fit to all of the data.

4.1. Capture yield and transmission plots

The capture and transmission data are plotted in Figs. 1–3 for the thermal measurement from 0.01 to 18 eV and in Figs. 4–6 for the epithermal measurements at the three s-wave ^{164}Dy resonances below 600 eV. Also plotted are the ENDF (Chadwick et al,

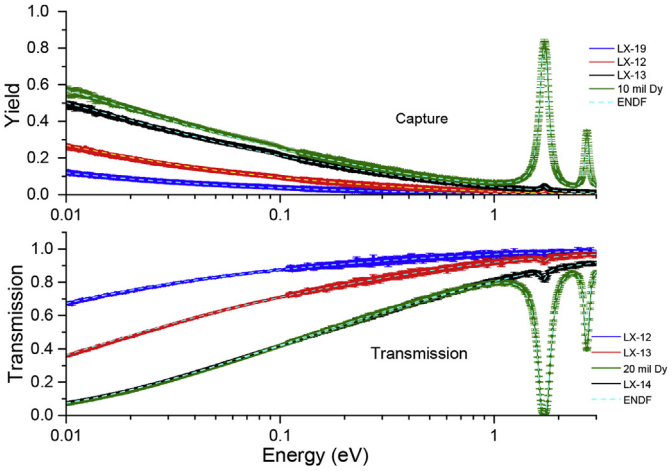

Fig. 1. Dy thermal capture and transmission from 0.01 to 3 eV.

Table 5
Capture detector efficiencies for the Dy isotopes with discriminator settings of 1 MeV and 2 MeV, respectively, for epithermal and thermal capture measurements.

Isotope	Binding energy (MeV)	Total energy disc. = 1 MeV (epithermal)	Total energy disc. = 2 MeV (thermal)
^{156}Dy	6.969	0.89 ± 0.03	0.83 ± 0.03
^{158}Dy	6.832	0.89 ± 0.02	0.83 ± 0.02
^{160}Dy	6.454	0.88 ± 0.02	0.82 ± 0.02
^{161}Dy	8.197	0.97 ± 0.02	0.91 ± 0.02
^{162}Dy	6.271	0.88 ± 0.02	0.81 ± 0.02
^{163}Dy	7.658	0.97 ± 0.02	0.89 ± 0.02
^{164}Dy	5.716	0.87 ± 0.03	0.78 ± 0.03

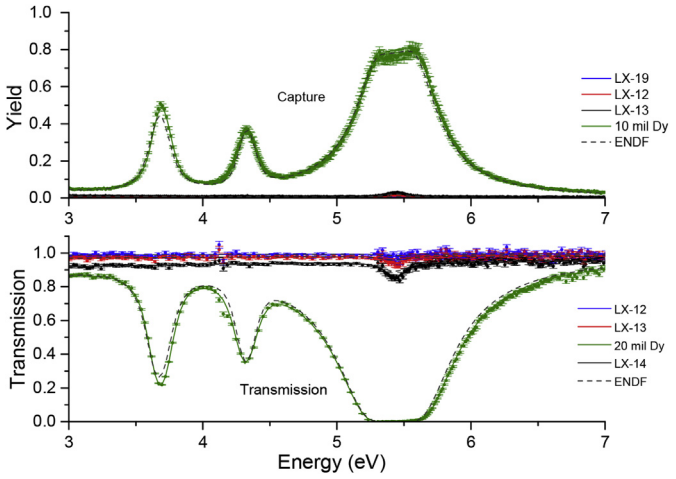

Fig. 2. Dy thermal capture and transmission from 3 to 7 eV.

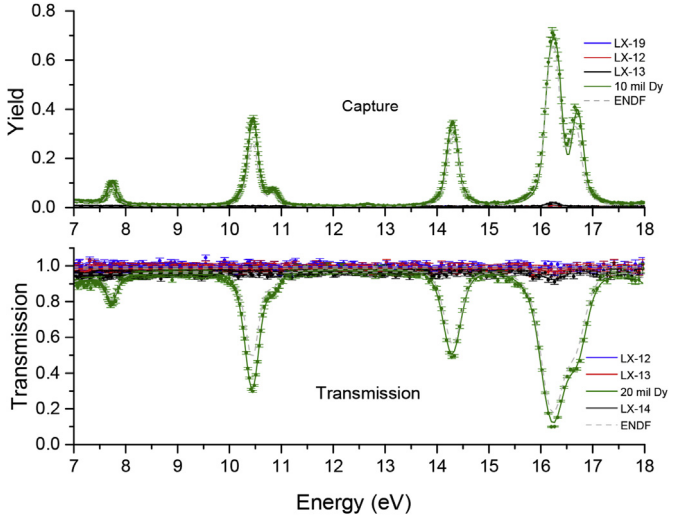

Fig. 3. Dy thermal capture and transmission from 7 to 18 eV.

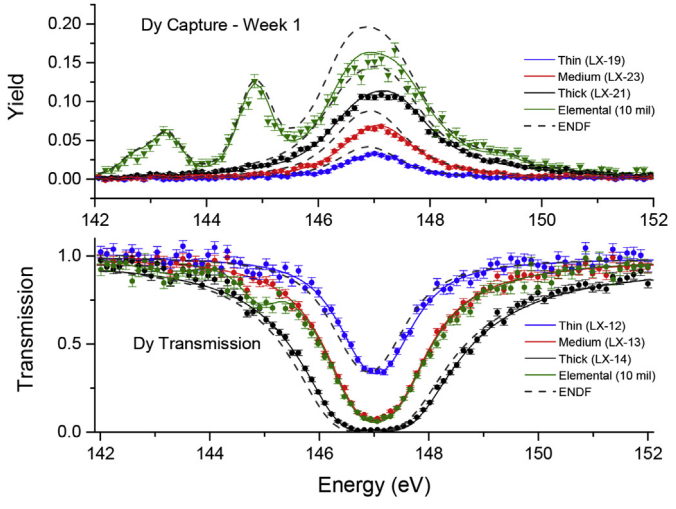

Fig. 4. Epithermal capture and transmission near the 147 eV ^{164}Dy resonance. The fits demonstrate a reduction in the radiation width relative to ENDF while the neutron width is nearly unchanged (see Table 6). Only the data for the first and third weeks of capture are shown. The slight rise in capture yield of the natural sample near 149 eV is attributed to multiple scattering and is calculated in the SAMMY fits.

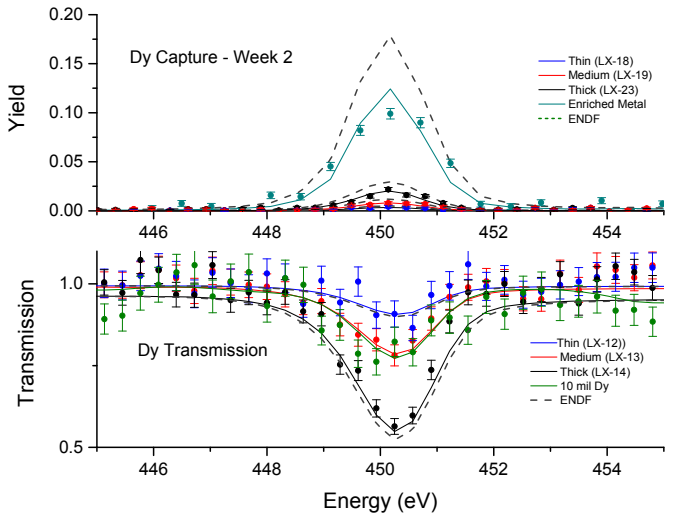

Fig. 5. Epithermal capture and transmission near the 450 eV resonance in ^{164}Dy. The fits demonstrate a reduction in the radiation width relative to ENDF while the neutron width is similar to that of ENDF (see Table 6). Only the data for the second week of capture are shown along with the metal sample enriched in ^{164}Dy.

2006) (dashed lines) and the SAMMY final fit (solid colored lines) to all of the data. Two weeks of epithermal capture data were taken with the liquid samples. For visual purposes only the capture data of week 1 for the 147 eV resonance and the week 2 capture data for the 450 and 536 eV resonances are plotted here; in each case, the other week's data are comparable in both statistics and accuracy of fit.

The final fits (solid lines) in these figures, for the most part, pass through the experimental data points. The ENDF plots (dashed lines) go through the majority of the thermal measurement data points, especially at the lower energies. For the epithermal plots there is a significant difference between the fits to this measurement and ENDF, especially in capture. There is some shift in energy between the final fit and ENDF values in these plots.

4.2. Resonance parameters

Table 6 summarizes the resonance parameters obtained from the transmission and capture data analysis. The thermal measurement was used to analyze all resonances up to 17 eV. Epithermal data alone were used to analyze the three large resonances in ^{164}Dy at 147, 450 and 536 eV. The negative energy resonances in ^{160}Dy and ^{163}Dy were set to ENDF resonance parameters and not varied. For the negative energy resonances in ^{161}Dy and ^{164}Dy the resonance energy and radiation widths were set equal to the ENDF values and only the neutron widths were allowed to vary. For resonances below ~10 eV, where the resolution width is small or comparable to the total width, the radiation width can be obtained from the SAMMY fit to the resonances. Above ~10 eV radiation widths were determined whenever a resonance included a significant quantity of scattering. The criterion of $\Gamma_\gamma/\Gamma_n < 5$ was adopted from Barry (Barry, 2003) to reflect sensitivity of a resonance to the value of its radiation width. For resonances with $\Gamma_\gamma/\Gamma_n > 5$ the radiation widths were set equal to their ENDF value for the SAMMY analysis.

In Table 6 the SAMMY resonance energy E_o, radiation width Γ_γ, and neutron width Γ_n are listed, respectively, in columns 1, 5 and 9. The corresponding ENDF resonance parameters $E_{o,endf}$, $\Gamma_{\gamma,endf}$ and $\Gamma_{n,endf}$ are listed in columns 4, 8 and 12. The SAMMY (Bayesian) absolute uncertainties in the resonance parameters $\Delta E_{o,B}$, $\Delta\Gamma_{\gamma,B}$ and

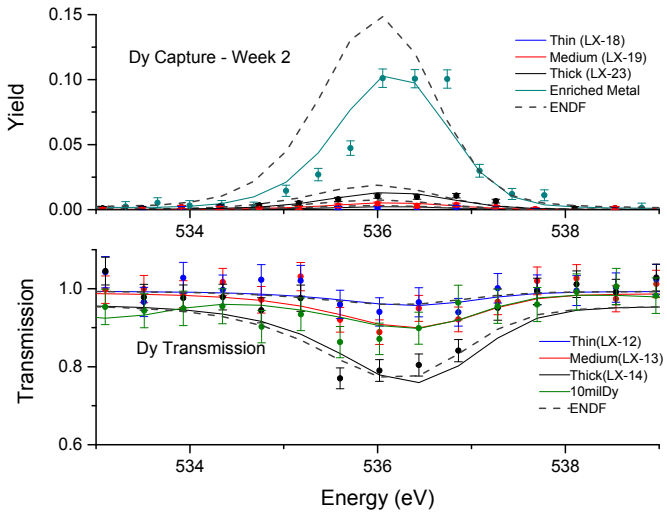

Fig. 6. Epithermal capture and transmission near the 536 eV resonance in ^{164}Dy. The fits demonstrate a reduction in the radiation width relative to ENDF while the neutron width is nearly unchanged (see Table 6). Only the data for the second week of capture are shown along with the metal sample enriched in ^{164}Dy.

$\Delta\Gamma_{n,B}$ are listed in columns 2, 6 and 10. The 'external' uncertainties $\Delta E_{o,ext}$, $\Delta\Gamma_{\gamma,ext}$ and $\Delta\Gamma_{n,ext}$ are listed in columns 3, 7 and 11.

External uncertainties are a measure of the fluctuations in the resonance parameters when each of the eight thermal measurements and each of the thirteen epithermal measurements are individually solved by SAMMY with the same input parameters. For the thermal measurement analysis the ENDF parameters were used as input (i.e., using ENDF parameters as the starting point for each Bayesian analysis). The final parameters from Ernesti (2008) were used as input for the epithermal measurement analysis.

The external uncertainty in E_o, Γ_γ, or Γ_n is determined from the mean-square-deviation Eq. (4).

$$\Delta X_{ext} = \sqrt{\left\{\sum_1^n \frac{(X_i - <X>_{ext})^2}{(\Delta X_{B,i})^2}\right\} \Big/ \left\{(n-1)\sum_1^n \frac{1}{(\Delta X_{B,i})^2}\right\}} \quad (4)$$

where X stands for E_o, Γ_γ, or Γ_n and n is the number of measurements (eight thermal or thirteen epithermal). The $\Delta X_{B,i}$ in Eq. (4) is the Bayesian SAMMY uncertainty in E_o, Γ_γ, or Γ_n for each sample i.

The average external parameter $<X>_{ext}$ in Eq. (4) is determined from Eq. (5).

$$<X>_{ext} = \sum_1^n \frac{X_i}{(\Delta X_{B,i})^2} \Big/ \sum_1^n \frac{1}{(\Delta X_{B,i})^2} \quad (5)$$

Note that there are large fluctuations in some of the external errors, some large and some small when compared to the SAMMY errors. SAMMY is a Bayesian analysis and for the initial input the resonance parameters were all assumed to have an uncertainty of ±10%. Thus, if the experimental data are such that the final parameters are essentially unchanged from the initial input parameters, the SAMMY final parameters will be very close to the initial input parameters and the variation in these output parameters will be very small. This leads to exceedingly small external errors. Therefore, external errors should be considered only significant when they are comparable to or greater than the SAMMY errors. It is recommended that the larger of these two errors be used in applying these results.

4.3. Thermal capture cross section and resonance integral

To determine the thermal capture cross section and resonance integral of ^{164}Dy, a set of data was prepared using a combination of the present data - the negative-energy resonance at −1.880 eV, the three positive energy resonances near 147, 450 and 536 eV, and the higher energy resonances from the ENDF evaluation. This set of data was input to the NJOY nuclear data processing code (MacFarlane and Muir, 1994) to obtain Doppler-broadened cross sections. From these cross sections the thermal capture cross section and capture resonance integral were computed. These results and the corresponding ENDF values are listed in Tables 7 and 8, respectively, for the ^{164}Dy thermal capture cross section and capture resonance integral. The capture resonance integral RI_γ was calculated from Eq. (6).

$$RI_\gamma = \int_{0.5eV}^{20\ MeV} \sigma_\gamma(E)\frac{dE}{E} \quad (6)$$

Table 6
The resonance parameters from the thermal and epithermal measurements. The subscripts B, ext, and endf refer, respectively, to final Bayesian uncertainties, external uncertainties and ENDF resonance parameters. The isotopic assignment and resonance spins J were taken from ENDF. For parameters that are not listed, the ENDF parameters were used for the SAMMY analysis.

E_o (eV)	$\Delta E_{o,B}$ (eV)	$\Delta E_{o,ext}$ (eV)	$E_{o,endf}$ (eV)	Γ_γ (meV)	$\Delta\Gamma_{\gamma,B}$ (meV)	$\Delta\Gamma_{\gamma,ext}$ (meV)	$\Gamma_{\gamma,endf}$ (meV)	Γ_n (meV)	$\Delta\Gamma_{n,B}$ (meV)	$\Delta\Gamma_{n,ext}$ (meV)	$\Gamma_{n,endf}$ (meV)	Iso	J
			−58.19				105.8				555.3	160	0.5
			−1.890				106.8	16	0.2	3	10.84	161	3
			−1.880				61.4	51.9	0.08	0.2	51.9	164	0.5
			−1.613				108.6				0.255	163	3
1.7190	0.0002	0.0002	1.713	90.6	0.3	0.2	102.6	2.229	0.009	0.007	2.040	163	2
2.7162	0.0003	0.0004	2.71	109.1	0.8	0.2	119.0	0.650	0.003	0.003	0.561	161	3
3.6920	0.0004	0.0006	3.68	111.6	0.7	0.1	124.0	2.30	0.01	0.02	2.136	161	2
4.3267	0.0006	0.0004	4.33	110	1	2	80.0	1.66	0.01	0.009	1.38	161	2
5.4489	0.0002	0.0006	5.44	104	0.4	1	147.4	28.7	0.06	0.2	21.10	162	0.5
7.734	0.007	0.001	7.74	133	6	3	107.0	0.62	0.02	0.008	0.514	161	3
10.24	0.006	0.02	10.26	120	10	1	106.8	0.24	0.01	0.002	0.288	161	2
10.4479	0.0005	0.0005	10.45	93	3	2	100.0	28.3	0.2	0.1	16.5	160	0.5
10.857	0.002	0.001	10.85				106.8	0.542	0.008	0.002	0.411	161	3
12.64	0.01	0.003	12.65				106.8	0.075	0.007	0.002	0.048	161	3
14.296	0.001	0.0005	14.31				124.0	8.99	0.05	0.01	7.44	161	2
16.2368	0.0006	0.0009	16.23				105.0	23.4	0.09	0.2	18.26	163	3
16.695	0.005	0.001	16.67				116.0	7.7	0.4	0.1	6.343	161	3
147.105	0.005	0.008	146.97	86	2	1	114.2	830	8	10	820	164	0.5
450.41	0.03	0.04	450.41	64	5	1	110	230	20	7	260	164	0.5
536.46	0.04	0.05	536.3	61	8	1	120	120	20	2	116	164	0.5

Table 7
The thermal capture cross section of ^{164}Dy obtained from this measurement and the ENDF evaluation.

Thermal capture cross section	
This experiment	ENDF
2980 ± 10 b	2981 b

Table 8
The capture resonance integral of ^{164}Dy obtained from this measurement and the ENDF evaluation.

Resonance integral	
This experiment	ENDF
338 ± 1 b	342.2 b

The errors listed in Tables 7 and 8 are based on the resonance parameter errors obtained in this experiment, i.e., the errors listed in Table 6. A Monte Carlo sampling method was employed to sample from these errors and to determine their impact on both the thermal capture cross section and resonance integral. For the past several years nuclear data scientists have been applying Monte Carlo methods to propagate uncertainties in nuclear data to reactor constants such as effective multiplication factors (k_{eff}), etc. (Rochman et al., 2014; Smith, 2008). In particular Rochman et al. used the Total Monte Carlo (TMC) method to propagate uncertainties in nuclear data to large scale nuclear reactor systems to obtain uncertainties in k_{eff} in critical benchmarks. The TMC is a brute force method that performs the same simulation repeatedly while sampling all parameters of interest from probability distributions for each simulation.

A particular set of ^{164}Dy resonance parameters was obtained by randomly selecting each resonance parameter from a normal distribution, centered about the central value from Table 6 and a 1σ width equal to the larger of the two uncertainties listed in Table 6. This set of randomly-selected resonance parameters, along with the ENDF parameters for the higher energy resonances, was then input to NJOY and new values of the thermal capture cross section and resonance integral were calculated. This process was repeated for many iterations (over 1000) to obtain the distribution of thermal capture cross sections and resonance integrals. The errors listed in Tables 7 and 8 are the 1σ errors for these two quantities.

The thermal capture cross section obtained in this experiment (Table 7) is practically identical to the ENDF value, so that the present result is a confirmation of the evaluated value. It is worth noting that the ^{164}Dy thermal capture cross section is dominated by the negative energy resonance which contributes to 99.96% of its value. The resonance integral from this experiment (Table 8) is about 1% smaller than the ENDF value.

5. Conclusions

Capture and transmission measurements were carried out with samples of natural Dy and samples of highly-enriched ^{164}Dy from 0.01 to over 600 eV. Resonance parameters were obtained for two negative-energy and 13 positive-energy Dy resonances below 18 eV and the three ^{164}Dy resonances at 147, 450 and 536 eV. The thermal capture cross section and resonance integral of ^{164}Dy determined from this measurement are very close to the ENDF values. However, the radiation widths of the three ^{164}Dy resonances at 147, 450 and 536 eV are all significantly smaller than the ENDF values. For these three resonances the average radiation width from this measurement is 61% of the average radiation width calculated from the ENDF parameters.

Acknowledgments

We thank the LINAC staff for both operating the accelerator during these measurements and providing us with the mechanical and electronic assistance we needed.

References

Barry, D.P., 2003. Neodymium Neutron Transmission and Capture Measurements and Development of a New Transmission Detector. Rensselaer Polytechnic Institute (PhD Thesis).

R.C. Block, P.J. Marano, N.J. Drindak, F. Feiner, K.W. Seemann, and R.E. Slovacek, "A Multiplicity detector for accurate low-energy neutron capture measurements," Proc. Int. Conf. Nuclear Data for Science and Technology, May 30-June 3, 1988, Mito, Japan, p. 383.

Chadwick, M.B., et al., 2006. ENDF/B-VII.1: next generation evaluated nuclear data library for science and technology. Nucl. Data Sheets 107 (12), 2931.

Danon, Y., Slovacek, R.E., Block, R.C., 1993. The enhanced thermal neutron target at the RPI LINAC. Trans. Am. Nucl. Soc. 68, 473.

Danon, Y., Slovacek, R.E., Block, R.C., 1995. Design and construction of a thermal neutron target for the RPI LINAC. Nucl. Instrum. Methods A 352, 596.

Ernesti, M.C., August 2008. Neutron Capture and Total Cross Section Measurements and Resonance Parameters for the 147 EV, 450 EV and 536 EV Resonances in 164Dy. University of Texas at Austin (MS thesis).

Kim, G., et al., 2003. Measurement of neutron total cross-section of Dy at Pohang neutron facility. Ann. Nucl. Energy 30, 1123.

Larson, N.M., October 2008. Updated User's Guide for SAMMY: Multilevel R-matrix Fits to Neutron Data Using Bayes Equations. Oak Ridge National Laboratory. ORNL/TM-9179/R8 ENDF-364/R2.

Leinweber, G., Barry, D.P., Burke, J.A., Rapp, M.J., Block, R.C., Danon, Y., Geuther, J.A., Saglime III, F.J., 2014. Europium resonance parameters from neutron capture and transmission measurements in the energy range 0.01-200 eV. Ann. Nucl. Energy 69, 74.

Liou, H.I., Hacken, G., Rainwater, J., Singh, U.N., 1975. Neutron resonance spectroscopy: the separated isotopes of Dy. Phys. Rev. C 11, 462.

MacFarlane, R., Muir, D., 1994. The NJOY Nuclear Data Processing System, Version 91. Los Alamos National Laboratory. LA-12740-M.

Moore, W., 1961. Bull. Am. Phys. Soc. 6, 70.

Mughabghab, S.F., Chrien, R.E., 1970. Study of radiation widths and neutron strength functions of the Dy isotopes. Phys. Rev. C 1, 1850.

Overberg, M.E., Moretti, B.E., Slovacek, R.E., Block, R.C., 1999. Photoneutron target development for the RPI linear accelerator. Nucl. Instrum. Methods A 438, 253.

Raaijmakers, W.A., 1965. The Treatment of Shaped Burnable Poisons in Analogue Burn-up Calculations. European Atomic Energy Community report EUR 2184.e.

Rochman, D., Zwermann, W., van der Marck, S., Koning, A., Sjörstrand, H., Helgesson, P., Krzykacz-Hausmann, B., 2014. Efficient use of Monte Carlo: uncertainty propagation. Nucl. Sci. Eng. 177, 337.

Sher, R., Tassan, S., Weinstock, E.V., 1961. Low energy neutron cross sections of Dy164. Nucl. Sci. Eng. 11, 369.

Smith, D., 2008. A Unified Monte Carlo Approach to Fast Neutron Cross Section Data Evaluation. Argonne National Laboratory. Tech. Rep. No.ANL/NDM-166.

Vertebnyj, V.P., Vlasov, M.F., Gnidak, N.L., Kiriljuk, A.L., Pavlenko, E.A., Pasechnik, M.V., Trofimova, N.A., Federov, A.F., 1971. Yaderno-fizicheskie Issledovaniya Reports, vol. 11, p. 59.

Wang, S., Lubert, M., Danon, Y., Francis, N.C., Block, R.C., Becvar, F., Kriticka, M., 2003. The RPI multiplicity detector response to γ-ray cascades following neutron capture in ^{149}Sm and ^{150}Sm. Nucl. Instrum. Methods A 513, 583.